

Article

Unified Fault-Tolerant Control and Adaptive Velocity Planning for 4WID-4WIS Vehicles under Multi-Fault Scenarios

Ao Lu * and Guangyu Tian

The State Key Laboratory of Intelligent Green Vehicle and Mobility, School of Vehicle and Mobility, Tsinghua University, Beijing 100084, China; tian_gy@tsinghua.edu.cn

* Correspondence: la21@mails.tsinghua.edu.cn

Abstract: Four-wheel independent drive and four-wheel independent steering (4WID-4WIS) vehicles provide increased redundancy in fault-tolerant control (FTC) schemes, enhancing heterogeneous fault-tolerant capabilities. This paper addresses the challenge of maintaining vehicle safety and maneuverability in the presence of actuator faults in autonomous vehicles, focusing on 4WID-4WIS systems. A novel unified hierarchical active FTC strategy is proposed to handle various actuator failures. The strategy includes an upper-layer motion controller that determines resultant force requirements based on trajectory tracking errors and a middle-layer allocation system that redistributes tire forces to fault-free actuators using fault information. This study, for the first time, considers multi-fault scenarios involving longitudinal and lateral coupling, calculating FTC boundaries for each fault type. Additionally, a fault tolerance index is introduced for 256 fault scenarios, using singular value decomposition to linearly represent the vehicle attainable force domain. Based on this, an adaptive velocity planning strategy is developed to balance safety and maneuverability under fault conditions. Matlab 2021a/Simulink and Carsim 2019 co-simulation results validate the proposed strategies, demonstrating significant improvements in fault-tolerant performance, particularly in complex and emergency scenarios.

Keywords: actuator faults; fault-tolerant control; 4WID-4WIS electric vehicles; velocity planning; attainable force domain



Citation: Lu, A.; Tian, G. Unified Fault-Tolerant Control and Adaptive Velocity Planning for 4WID-4WIS Vehicles under Multi-Fault Scenarios. *Actuators* **2024**, *13*, 407. <https://doi.org/10.3390/act13100407>

Academic Editor: Cristina Morel

Received: 21 August 2024

Revised: 26 September 2024

Accepted: 30 September 2024

Published: 7 October 2024



Copyright: © 2024 by the authors. Licensee MDPI, Basel, Switzerland. This article is an open access article distributed under the terms and conditions of the Creative Commons Attribution (CC BY) license (<https://creativecommons.org/licenses/by/4.0/>).

1. Introduction

Recently, the rapid development of intelligent and autonomous vehicles has sparked growing interest in advanced vehicle control techniques, enhancing road traffic safety and efficiency. However, when key actuators experience faults, vehicles may lose stability and pose significant risks as drivers gradually withdraw from driving activities, especially when timely stopping is not feasible. Such scenarios can lead to sudden lane deviations and collisions with surrounding vehicles, increasing accident risks as vehicle stability deteriorates [1]. Therefore, fault-tolerant control (FTC) is critically important. FTC strategies aim to minimize or prevent the impact of faults in highly reliable control systems, ensuring the stable operation and acceptable performance of autonomous vehicles under various fault conditions. FTC approaches are generally classified into passive FTC and active FTC. Passive FTC relies mainly on the system's inherent robustness to handle specific faults and uncertainties [2–4]. In contrast, active FTC involves a fault diagnosis system to detect and isolate faults, and then, the controller is reconfigured based on fault information, making it more effective in addressing various fault types [5–8].

Currently, four-wheel independent drive and four-wheel independent steering (4WID-4WIS) vehicles, known for their advantages in rapid torque response, flexible control, chassis integration, and superior maneuverability, have become a research hotspot for major automotive manufacturers and academic institutions globally, recognized as the optimal platform for advanced vehicle dynamics control [9]. These vehicles feature four independent drive and steering motors, allowing the individual control of each wheel's

drive and steering. Compared to traditional vehicles, they offer more redundancy for FTC schemes and enhance heterogeneous fault-tolerant capabilities. Moreover, this configuration extends the boundaries of vehicle dynamics control, enabling high maneuverability even in cases of complete actuator failure, which is crucial for applications in emergency response and some specialized vehicles. Actuator failures typically involve drive, brake, and steering systems, but since drive and brake failures similarly affect longitudinal torque output, this paper focuses on drive and steering actuator failures. When a drive or steering actuator fails completely, resulting in zero drive torque or wheel steering angle, the situation becomes highly dangerous. This may lead to sudden lane departure and collisions with nearby vehicles, increasing the risk of accidents as vehicle stability deteriorates.

In the cases of actuator failures, most existing research focuses primarily on developing FTC strategies for single fault types. Cui et al. [10] primarily considered brake actuator faults, designing a path-tracking H_∞ fault-tolerant controller that adjusts fault coefficients based on the fault type to reallocate braking pressure. Zhu et al. [11] proposed a fault-tolerant controller that reconstructs motor drive torque to maintain vehicle stability by providing fault-free motor output based on fault diagnosis. Deng et al. [12] developed a torque distribution method based on reinforcement learning to address single-wheel drive actuator faults. Dai et al. [13] introduced an FTC method using the meta deep deterministic policy gradient algorithm to adapt to different fault scenarios by selecting the most suitable meta-trained model. When a single-wheel drive fails completely, torque vectoring can maintain vehicle stability by redistributing torque. However, as the number of drive actuator failures increases, torque vectoring becomes insufficient to provide the necessary yaw moment for stability. In such cases, developing an FTC strategy that leverages the remaining functional steering actuators would be an effective approach, but there has been little in-depth research on these specific scenarios. Mihály and Gáspár [14] designed a hierarchical controller that reallocates longitudinal tire forces to generate additional yaw moments in the event of front-axle steering failures. To address single-wheel steering failures, Zhang et al. [15] developed an active FTC system using a PI controller in the upper layer to calculate total force demand, while optimally distributing longitudinal and lateral tire forces through linear quadratic programming. Liu et al. [16] used a Linear Quadratic Regulator (LQR) controller to calculate the total force demand, and the tire forces were redistributed using a pseudo-inverse method while considering road adhesion constraints. When a single-wheel steering actuator fails completely, torque vectoring through the functional drive actuators or rear-wheel steering can maintain steering. However, as the number of steering actuator failures increases, or in cases where both drive and steering actuators fail simultaneously, the fault scenarios become significantly more complex. Few studies have explored these scenarios in depth, as existing research is often limited to single fault types or subsystems, overlooking the impact of multiple, complex failures, especially those involving simultaneous failures in both drive and steering systems with lateral and longitudinal coupling. Therefore, we comprehensively investigate these coupled fault scenarios and propose fault-tolerant measures, leveraging the heterogeneous fault-tolerant capabilities of 4WID-4WIS vehicles.

For velocity planning, most existing studies focus on velocity planning under normal vehicle conditions. Zhu et al. [17] proposed a velocity planning strategy based on reinforcement learning, considering safety, comfort, and efficiency. Herrmann et al. [18] introduced a velocity optimization algorithm at the handling limits, accounting for variable friction coefficients to reduce energy consumption and power losses. However, as actuator faults increase, the attainable FTC domain diminishes, increasing the likelihood of exceeding vehicle performance limits and degrading control performance. This suggests that control targets after a malfunction may need to be lower than those in fault-free conditions, requiring a reduction in acceptable performance to ensure safety, necessitating the replanning of driving velocity. Few existing studies consider velocity planning with FTC, particularly in balancing safety and maneuverability across various fault situations.

Therefore, this paper aims to conduct an in-depth analysis of multiple faults and their fault-tolerant strategies, clarifying fault-tolerant boundaries and capabilities under various fault conditions. We determine these boundaries to provide important references for enhancing driving safety and high maneuverability, especially in complex and emergency scenarios. Based on this, an adaptive velocity planning (AVP) strategy is proposed. The main contributions of this paper are summarized as follows:

- (1) A novel unified hierarchical active FTC strategy is proposed for various actuator failure scenarios. The resultant force requirements are determined by the upper-layer motion controller based on trajectory tracking errors, while tire forces are reallocated by the middle layer to the lower-layer fault-free actuators based on fault information.
- (2) The multi-fault situation involving longitudinal and lateral coupling is considered for the first time, with all possible fault types covered. The FTC boundaries for each fault scenario are calculated, providing important references for FTC design.
- (3) A fault tolerance index is innovatively proposed, capable of linearly representing the vehicle attainable force domain using singular value decomposition (SVD). Based on this, an AVP strategy is introduced that comprehensively considers safety and maneuverability under fault conditions.

The remainder of this paper is organized as follows: Section 2 presents the dynamic models, including vehicle, tire, and trajectory tracking models. Section 3 details the unified hierarchical fault-tolerant controller design. Section 4 discusses the vehicle attainable force domain under various fault types and the AVP strategy. Section 5 provides simulation results and analysis under all fault types. Section 6 concludes the paper.

2. Dynamic Model

2.1. Vehicle Dynamic Model

To effectively illustrate the advantages of 4WID-4WIS vehicles, we develop a double-track vehicle dynamic model with seven degrees of freedom (7-DOF), as depicted in Figure 1. The longitudinal, lateral, and yaw motions and 4-wheel dynamics are described as follows:

$$\begin{aligned} \Sigma F_x - mgf - \frac{1}{2}C_D A \rho v_x^2 &= ma_x = m(\dot{v}_x - \omega_r v_y) \\ \Sigma F_y &= ma_y = m(\dot{v}_y + \omega_r v_x) \\ \Sigma M_z &= I_z \dot{\omega}_r \\ T_{di} - T_{bi} - f_{xi} r &= I_{wi} \dot{\omega}_i, i = fl, fr, rl, rr \end{aligned} \quad (1)$$

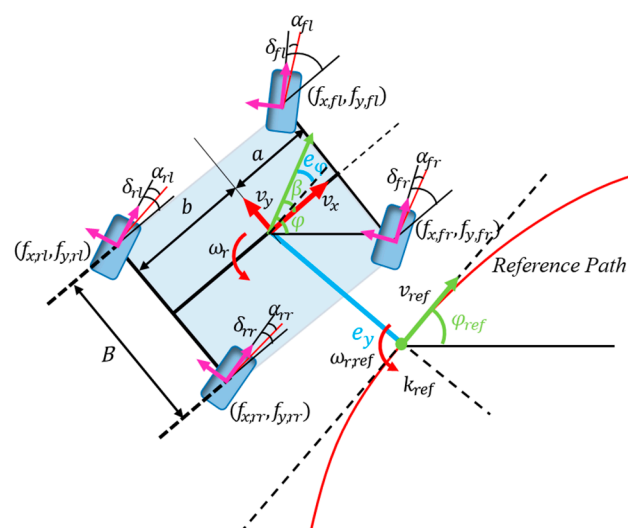


Figure 1. The vehicle dynamic model and the trajectory tracking model.

In the equation, m represents the vehicle's mass, g is the acceleration due to gravity, f is the rolling resistance coefficient, C_D is the air drag coefficient, ρ is the air density, and A

denotes the vehicle's frontal area. The longitudinal and lateral velocities are indicated by v_x and v_y , respectively, while a_x and a_y represent the longitudinal and lateral accelerations. The yaw rate is denoted by ω_r . I_z signifies the vehicle's yaw inertia about its center of gravity (CG). I_{wi} is the rotational inertia of each wheel and its drivetrain. The wheel's rotational speed is represented by ω_i . T_{di} and T_{bi} are the drive and braking torques, respectively. r is the effective rolling radius of the tire, and f_{xi} denotes the longitudinal forces of the front left tire, front right tire, rear left tire, and rear right tire by $i = fl, fr, rl, rr$. Moreover, the total longitudinal force, lateral force, and yaw moment are separately represented by $\sum F_x$, $\sum F_y$, and $\sum M_z$.

2.2. Tire Model

Since the longitudinal and lateral tire forces are essential for determining the actuator input, it is important to account for the nonlinear characteristics of tires, especially combined slip and the reduction in the coefficient of friction with increased sliding speed. To illustrate this nonlinear tire behavior, the following combined-slip brush tire model proposed by Pacejka [19] is employed:

$$\begin{aligned} f_x &= \frac{K_s}{\gamma_t} \left(\frac{\kappa}{1+\kappa} \right) f, f_y = \frac{-K_\alpha}{\gamma_t} \left(\frac{\tan \alpha}{1+\kappa} \right) f \\ \gamma_t &= \sqrt{K_s^2 \left(\frac{\kappa}{1+\kappa} \right)^2 + K_\alpha^2 \left(\frac{\tan \alpha}{1+\kappa} \right)^2} \\ f &= \begin{cases} \gamma_t - \frac{1}{3\mu f_z} \gamma_t^2 + \frac{1}{27\mu^2 f_z^2} \gamma_t^3, & (\gamma_t \leq 3\mu f_z) \\ \mu f_z, & (\gamma_t > 3\mu f_z) \end{cases} \end{aligned} \quad (2)$$

In the equation, K_s and K_α represent the tire's longitudinal stiffness and cornering stiffness, respectively. κ denotes the tire's slip rate, while α indicates the tire slip angle. μ stands for the road surface adhesion coefficient.

2.3. Trajectory Tracking Model

Trajectory tracking control involves independently managing the vehicle's movement in three directions: longitudinal, lateral, and yaw. These correspond to the vehicle velocity v , sideslip angle β , and yaw rate ω_r , as shown in Figure 1. Additionally, the vehicle course rate $\dot{\varphi}$ is related to the vehicle states as follows:

$$\dot{\varphi} = \dot{\beta} + \omega_r \quad (3)$$

when tracking the reference trajectory, the task is transformed into controlling the target states to approach zero as quickly as possible, including minimizing the velocity error e_v , sideslip angle tracking error e_β , and course angle tracking error e_φ , which encompass all planar motion information. These errors are defined as follows:

$$\begin{aligned} e_v &= v - v_{ref} \\ e_\beta &= \beta - \beta_{ref} \\ e_\varphi &= \varphi - \varphi_{ref} \end{aligned} \quad (4)$$

In the equation, v_{ref} , β_{ref} , and φ_{ref} represent the target vehicle velocity, sideslip angle, and course angle of the reference trajectory, respectively. To further improve tracking performance, the lateral tracking error e_y is used, which can be calculated as follows:

$$\begin{aligned} \dot{e}_y &= v \sin(e_\varphi) \approx v e_\varphi \\ \ddot{e}_y &\approx v \dot{e}_\varphi + \dot{v} e_\varphi \\ \dot{e}_\varphi &= \dot{\varphi} - \dot{\varphi}_{ref} = \dot{\varphi} - k_{ref} \left(\frac{v \cos(e_\varphi)}{1 - k_{ref} e_y} \right) \end{aligned} \quad (5)$$

In the equation, k_{ref} denotes the curvature of the target trajectory, indicating that the vehicle can use course rate $\dot{\varphi}$ and velocity rate \dot{v} to reduce path deviation. According to

Equation (3), the course rate can be converted into control of the vehicle sideslip angle rate and yaw rate.

3. Unified Fault-Tolerant Control Design

In over-actuated systems, control allocation is a common strategy [20] and is particularly useful for compensating during actuator failures. The control framework consists of three layers, as shown in Figure 2. The upper-layer motion controller determines the overall force requirements for trajectory tracking. The middle-layer control allocation redistributes tire force control to the lower-layer fault-free actuators based on the actuator fault information from the fault diagnosis. The lower layer is responsible for executing the commands, ensuring precise application of the necessary forces to maintain vehicle stability and performance.

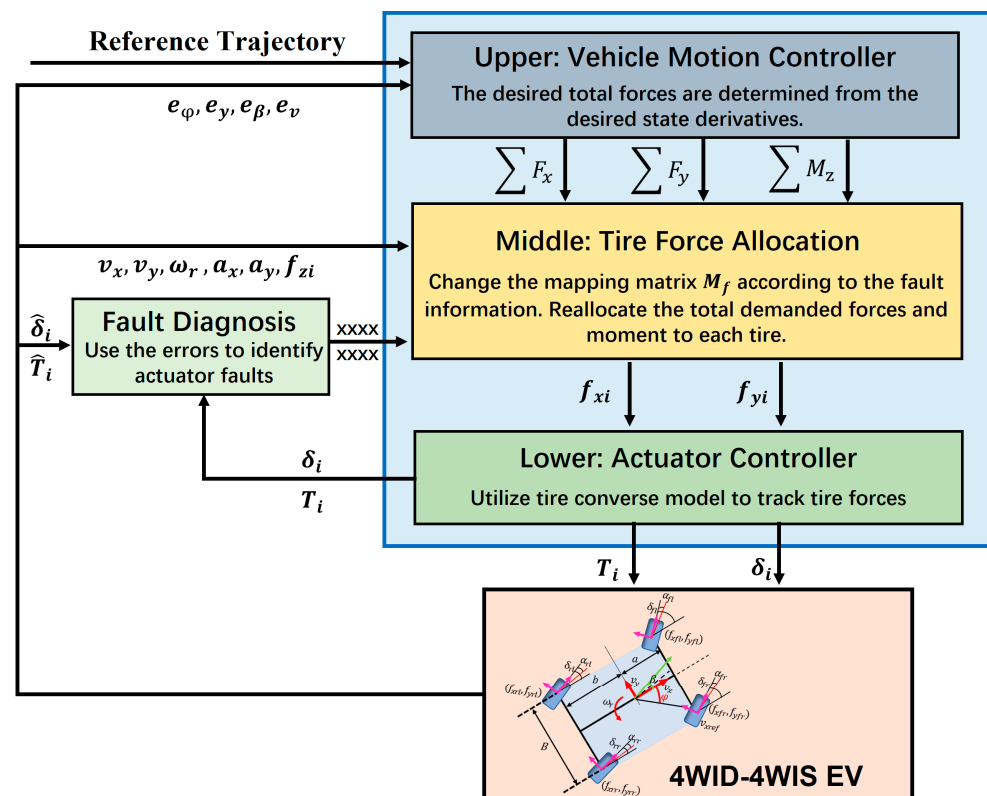


Figure 2. The hierarchical architecture of unified FTC.

3.1. Vehicle Motion Control

The upper-level motion control layer is algorithmically flexible, allowing for the application of any appropriate feedback control laws. As this is not the main focus of our study, we employ a linear control law to determine the desired total forces based on trajectory tracking errors [21]. The linear feedback control law is defined as follows:

$$\begin{aligned} \ddot{e}_y &= -k_p e_y - k_d \dot{e}_y \\ \dot{e}_\beta &= -k_\beta e_\beta \\ \dot{e}_v &= -k_v e_v \\ \dot{\omega}_{r,des} &= -k_r (\omega_r - \omega_{r,syn}) + \dot{\omega}_{r,syn} \end{aligned} \quad (6)$$

In the equation, k_p and k_d are the proportional and derivative gains for lateral tracking error, while k_β , k_v and k_r are the gains for sideslip angle tracking, velocity tracking, and yaw rate tracking, respectively. $\omega_{r,syn}$ and $\omega_{r,des}$ denote the synthetic and desired yaw rates. Given the minimal derivative of the reference vehicle velocity \dot{v}_{ref} , Equations (5) and (6)

allow us to approximate the course rate error \dot{e}_φ , the synthetic yaw rate $\omega_{r,syn}$, and the synthetic yaw acceleration $\dot{\omega}_{r,syn}$ as follows:

$$\begin{aligned}\dot{e}_\varphi &\approx \left(-\frac{k_p}{v}e_y - k_d e_\varphi\right) \\ \omega_{r,syn} &\approx \left(-\frac{k_p}{v}e_y - k_d e_\varphi\right) + k_\beta e_\beta + \omega_{r,ref} \\ \dot{\omega}_{r,syn} &\approx \left(\frac{k_p}{v^2} + \frac{k_p k_d}{v}\right)e_y + (k_d^2 - k_p)e_\varphi - k_\beta^2 e_\beta + \dot{\omega}_{r,ref}\end{aligned}\quad (7)$$

Using Equations (6) and (7), the desired total longitudinal force, lateral force, and yaw moment in the vehicle body-frame dynamics can be calculated from the desired state derivatives as follows:

$$\begin{aligned}\sum F_x &= m(-k_v e_v) \cos(\beta) - \left(mv\left(-\frac{k_p}{v}e_y - k_d e_\varphi\right) + \dot{\varphi}_{ref}\right) \sin(\beta) \\ \sum F_y &= m(-k_v e_v) \sin(\beta) + \left(mv\left(-\frac{k_p}{v}e_y - k_d e_\varphi\right) + \dot{\varphi}_{ref}\right) \cos(\beta) \\ \sum M_z &= I_z(-k_r(\omega_r - \omega_{r,syn}) + \dot{\omega}_{r,syn})\end{aligned}\quad (8)$$

3.2. Fault Diagnosis and Tire Force Reallocation

Complete actuator failures result in deviations from the target control values. In the 4WID-4WIS system, failures are categorized based on wheel position. For clarity, actuators are divided into front and rear axles, with the left-wheel drive actuator, steering actuator, right-wheel drive actuator, and steering actuator arranged from left to right. The fault diagnosis system compares control target values from the control algorithm with the actual wheel torques or steering angles measured by sensors. The resulting errors are used to detect actuator failures, with significant discrepancies indicating a fault. The state of each actuator is indicated by X (0 or 1), where 1 denotes a functional actuator and 0 indicates a complete failure. This fault information is used as a key reference for tire force reallocation, as shown in Figure 2. With eight actuators (four drive and four steering), there are a total of 255 possible fault combinations.

At the middle level, the total required forces and moment are allocated to each tire using constrained optimization. The total forces are derived from the contributions of the four tires as follows:

$$\begin{aligned}\sum F &= M_f f \\ \sum F &= [\sum F_x, \sum F_y, \sum M_z]^T \\ M_f &= \begin{bmatrix} \cos \delta_{fl} & \sin \delta_{fl} & -\frac{B}{2} \cos \delta_{fl} + a \sin \delta_{fl} \\ -\sin \delta_{fl} & \cos \delta_{fl} & a \cos \delta_{fl} + \frac{B}{2} \sin \delta_{fl} \\ \cos \delta_{fr} & \sin \delta_{fr} & \frac{B}{2} \cos \delta_{fr} + a \sin \delta_{fr} \\ -\sin \delta_{fr} & \cos \delta_{fr} & a \cos \delta_{fr} - \frac{B}{2} \sin \delta_{fr} \\ \cos \delta_{rl} & \sin \delta_{rl} & -\frac{B}{2} \cos \delta_{rl} - b \sin \delta_{rl} \\ -\sin \delta_{rl} & \cos \delta_{rl} & -b \cos \delta_{rl} + \frac{B}{2} \sin \delta_{rl} \\ \cos \delta_{rr} & \sin \delta_{rr} & \frac{B}{2} \cos \delta_{rr} - b \sin \delta_{rr} \\ -\sin \delta_{rr} & \cos \delta_{rr} & -b \cos \delta_{rr} - \frac{B}{2} \sin \delta_{rr} \end{bmatrix}^T \\ f &= [f_{xfl}, f_{yfl}, f_{xfr}, f_{yfr}, f_{xrl}, f_{yrl}, f_{xrr}, f_{yrr}]^T\end{aligned}\quad (9)$$

In the equation, f_{xi} , f_{yi} , and δ_i represent the longitudinal force, lateral force, and wheel steering angle for each tire, respectively, with $i = fl, fr, rl, rr$ denoting the front left, front right, rear left, and rear right tires. The variables a and b indicate the distances from the CG to the front and rear axles, respectively, while B represents the wheel track width. The primary objective of optimization is to meet the total control requirements, considering

road adhesion and actuator limits. Additionally, the optimization seeks to minimize total tire adhesion utilization. The optimization objective J_z can be described as follows:

$$J_z = \min(\|k_\gamma W_f f\|_2^2 + \|W_F(\Sigma F - M_f f)\|_2^2) \quad (10)$$

$$W_f = \text{diag}(\frac{1}{\mu_{f_{zfl}}}, \frac{1}{\mu_{f_{zfr}}}, \frac{1}{\mu_{f_{zrl}}}, \frac{1}{\mu_{f_{zrr}}})$$

$$\sqrt{f_{xi}^2 + f_{yi}^2} \leq \mu_{f_{zi}}$$

In the equation, k_γ is a weighting factor, and W_F is a diagonal matrix containing weight coefficients. The friction circle constraints transform the control allocation into a quadratically constrained quadratic programming (QCQP) problem, which can increase computational demands due to longer computation times. To streamline optimization and enhance computational efficiency [22], the friction circle constraints are often approximated by a linear octagon, converting the trajectory tracking control into a constrained optimal tire force allocation problem, making it a quadratic programming (QP) problem. The active-set algorithm is used due to its efficiency in computation.

With a hierarchical control allocation framework, a unified fault-tolerant controller can be developed to handle various actuator failures. It involves adjusting M_f based on fault information, setting the output torque or steering angle of the faulty actuator to 0 as equation constraints, while maximizing the use of other operational actuators to maintain acceptable performance.

3.3. Actuator Control

At the lower level, the calculated tire forces are achieved through each wheel's torque and steering angle. The wheel driving/braking torque, derived from each tire's longitudinal force as shown in Equation (1), is limited by the drive motor. Since drive and brake failures similarly affect the longitudinal torque output, this paper focuses only on drive and steering actuator failures. The steering angles for all four wheels are given by the following:

$$\delta_{fl} = \tan^{-1}\left(\frac{v_y + a\omega_r}{v_x - \frac{b}{2}\omega_r}\right) - \alpha_{fl}, \quad \delta_{fr} = \tan^{-1}\left(\frac{v_y + a\omega_r}{v_x + \frac{b}{2}\omega_r}\right) - \alpha_{fr} \quad (11)$$

$$\delta_{rl} = \tan^{-1}\left(\frac{v_y - b\omega_r}{v_x - \frac{b}{2}\omega_r}\right) - \alpha_{rl}, \quad \delta_{rr} = \tan^{-1}\left(\frac{v_y - b\omega_r}{v_x + \frac{b}{2}\omega_r}\right) - \alpha_{rr}$$

In the equation, α_i represents the slip angle of each tire, obtained through the tire inverse model. The wheel steering angle range adheres to the physical constraints of the steering system. When a wheel steering actuator fails and the actual steering angle is zero, the lateral force still remains non-zero. Using velocity and yaw rate data, the tire slip angle can be calculated from Equation (11). This calculation allows for the estimation of the affected lateral tire force, which is then incorporated as a constraint in the tire force control allocation, effectively isolating the faulty wheel from steering control.

4. Adaptive Velocity Planning

The vehicle attainable force domain is fundamentally determined by the tire's force capabilities. As actuator faults become more varied and interconnected, the range of FTC decreases, impacting the vehicle's performance limits. In situations where the vehicle encounters severe malfunctions or excessive lateral acceleration during trajectory tracking, merely reconfiguring the controller may not restore original control performance. In such cases, it is necessary to sacrifice some performance to ensure safety while maintaining acceptable control performance. Thus, we propose an AVP strategy based on the attainable force domain to ensure effective FTC.

4.1. Calculation of Attainable Force Domain

The vehicle attainable force domain effectively represents the system's force or moment limits and is crucial for analyzing performance constraints from a dynamics perspective. Considering the vehicle's steering performance, power characteristics, and road conditions,

the tire adhesion constraints are used to represent the influence of various factors and are converted into the vehicle attainable force domain, i.e., the coupled total force constraints in three directions, based on which, velocity planning is conducted. The brute force method (BFM) is a commonly used technique for calculating this domain [23,24]. Therefore, we employ the BFM to determine the vehicle attainable force volume under various fault conditions and to compute the volume ratio compared to the fault-free condition, as depicted in Figure 3. Generally, the vehicle attainable force volume decreases as the number of actuator faults increases. When there are seven or more actuator failures, the volume drops to zero, rendering the entire vehicle control ineffective and unable to steer or drive normally. With six actuator failures, the remaining two control inputs result in a volume ratio of zero, making it impossible to control longitudinal, lateral, and yaw directions simultaneously.

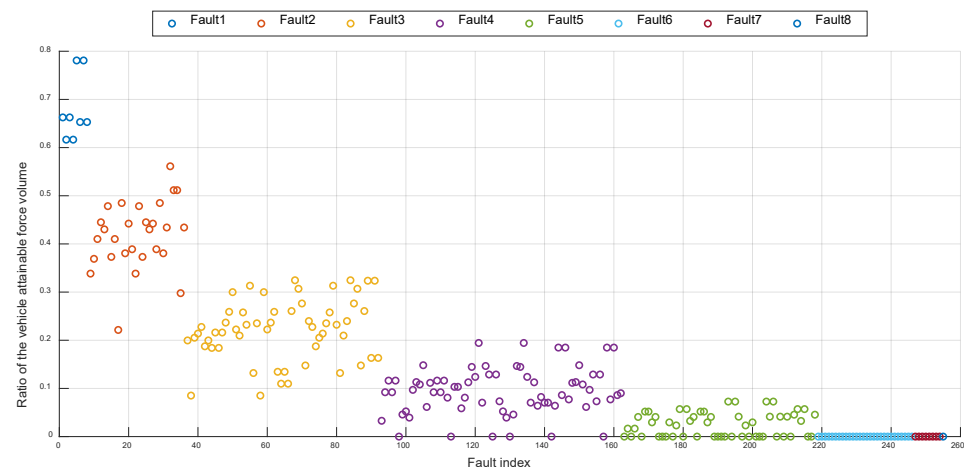


Figure 3. The ratio of vehicle attainable force volumes under different numbers of faults. The fault index is arranged in lexicographical order from 1 to 255, based on the number of faults and the order of actuators, from smallest to largest.

4.2. Velocity Planning Based on Fault Tolerance

Although we have calculated the vehicle attainable force volume for all fault scenarios, using the BFM to determine the force domain under multiple fault states remains complex, time-consuming, and unsuitable for real-time applications. Therefore, we propose using the singular value of the transition matrix in Equation (9) to represent the scaling size, which can characterize the vehicle attainable force volume. SVD is straightforward to calculate and suitable for real-time applications. We use the squared product of singular values to characterize the fault tolerance and normalize the fault tolerance index compared to the non-fault state, as follows:

$$G = \det \left(M_f M_{f_z} \left(M_f M_{f_z} \right)^T \right) = (\sigma_1 \sigma_2 \sigma_3)^2 \quad (12)$$

$$M_{f_z} = \text{diag} \left[\mu f_{zfl}, \mu f_{zfr}, \mu f_{zrl}, \mu f_{zrr} \right]$$

In the equation, σ_1 , σ_2 , and σ_3 are the corresponding singular values. The fault tolerance index G is then substituted into the attainable force volume V_F under static loads, as shown in Figure 4. The Pearson correlation coefficient between G and V_F is $R = 0.986$, $p < 0.001$, indicating an excellent fit. Moreover, all faults with an attainable force volume of zero are accurately represented by the fault tolerance index.

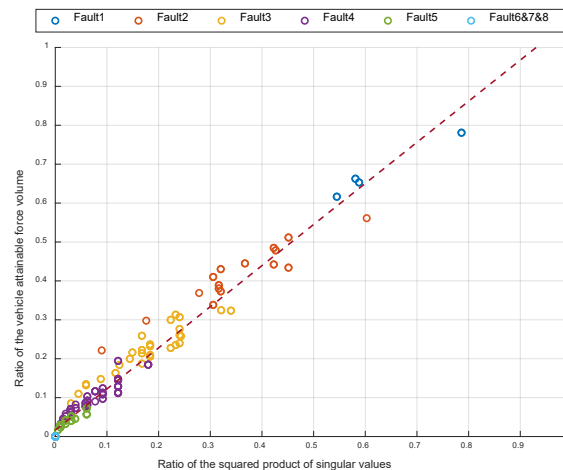


Figure 4. Fitting results of the attainable force volume ratio and the fault tolerance index under static load conditions for various vehicle fault states.

Consequently, we propose an FTC strategy that adaptively adjusts the target vehicle speed based on the degree of actuator failure, balancing handling stability and maneuverability. The target vehicle velocity is defined as follows:

$$v_{ref} = \frac{v_0(1 + \sqrt{G})}{2} \quad (13)$$

In the equation, v_0 is a preselected standard speed, chosen as the maximum speed that can safely track the reference trajectory under non-fault conditions.

5. Simulation Results and Analysis

To demonstrate the efficiency of the FTC strategy developed in this work and its ability to ensure normal vehicle operation under various actuator faults, we perform joint simulations using Matlab 2021a/Simulink and Carsim 2019, focusing on a 4WID-4WIS EV with parameters listed in Table 1. We compare the performance of a double lane change (DLC) maneuver under four conditions, no FTC, FTC, FTC-Comparison and FTC-AVP, across different fault types. An existing FTC method in [16] uses LQR to compute the desired total forces and moment, and the tire forces are redistributed using a pseudo-inverse method. This method is used for comparison to verify the superiority of the proposed method. Additionally, the initial target speed is set to 80 km/h, and the road surface adhesion coefficient is set to 1.

Table 1. Parameters of the 4WID-4WIS EV model.

Parameter	Symbol	Value
Vehicle mass	m	1230 kg
Vehicle yaw inertia	I_z	1343.1 kg·m ²
CG to front axle	a	1.06 m
CG to rear axle	b	1.54 m
Tire effective rolling radius	r	0.298 m
Wheel track width	B	1.48 m

5.1. Analysis in Specific Scenarios

We consider complete steering and drive actuator failures for a 4WID-4WIS vehicle, with eight actuators (four steering and four drive) on the front and rear axles, resulting in 255 possible fault types, excluding the normal condition without actuator failure for comparison, with each fault numerically labeled. For clarity, we use numbers 1 to 8 to sequentially represent the fault status of the drive and steering actuators from left to right

on the front and rear axles. For example, “fault 1-2-7-8” indicates complete failure of the drive and steering actuators in the front left and rear right wheels, while those in the front right and rear left wheels remain functional. Additionally, actuator failures are assumed to occur at the beginning to validate the effectiveness of the control strategy. For in-depth analysis, we select one specific fault type: front-axle drive failure combined with front right-wheel steering failure, referred to as “fault 1-3-4”, where three actuators fail simultaneously. The results of the DLC trajectory tracking control are shown in Figure 5.

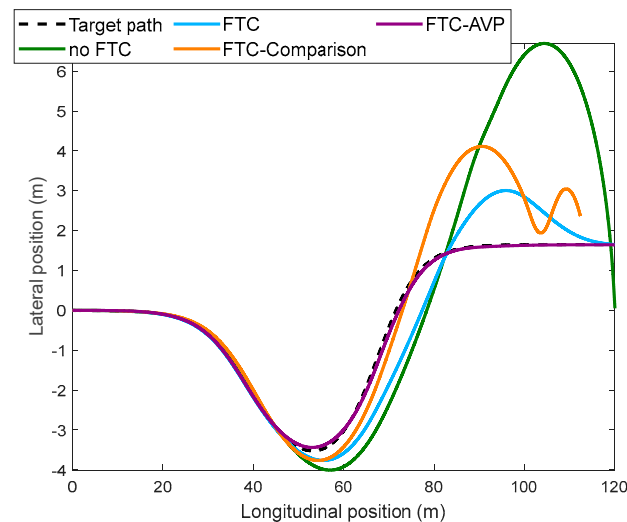


Figure 5. Tracking performance in DLC under fault 1-3-4.

The results indicate that when both the steering and drive actuators fail simultaneously, vehicles without FTC may lose stability, posing a serious safety risk. The referenced FTC strategy also struggles to maintain trajectory tracking, leaving the vehicle in an unstable state at the end. In contrast, the proposed FTC can stabilize the vehicle and prevent loss of control. However, at high driving speeds, actuator malfunctions reduce the vehicle attainable force range, exceeding its boundary and resulting in a maximum trajectory tracking error of 1.368 m. Our AVP strategy, based on the fault tolerance index using SVD, demonstrates excellent trajectory tracking performance. Figures 6 and 7 show that the course angle and sideslip angle tracking errors under the referenced FTC are significantly large, with the vehicle remaining unstable. Without AVP, the proposed FTC achieves stability, but the tracking angle errors are still greater than those under the proposed FTC with AVP. The maximum course angle and sideslip angle tracking errors under FTC-AVP are both within 4 degrees, representing the best performance. This is because, at excessively high target speeds, vehicle control may exceed its fault tolerance range, making it difficult to achieve the same control effect as in a fault-free state.

Figures 8 and 9 illustrate the four-wheel torque and steering angle commands under the four control strategies. When actuator failure occurs without corresponding FTC, incorrect torque and angle commands are generated, as shown in Figures 8a,b and 9b, leading to serious control mismatches and vehicle instability. Under the proposed FTC strategy, acceptable control is achieved by fully utilizing the still-functional actuators through controller reconfiguration and isolating the faulty actuators. As shown in Figure 8c,d, during the lane change process, the still-functional rear-wheel torque is fully utilized for torque vectoring control, generating a yaw moment that aids vehicle steering and maintains stability.

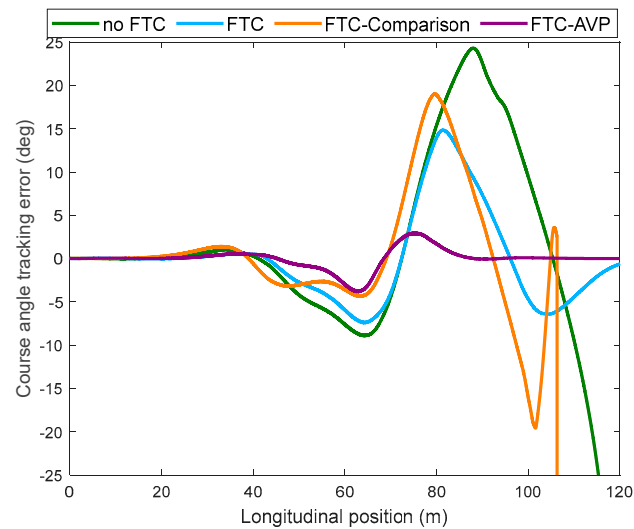


Figure 6. Course angle tracking error in DLC under fault 1-3-4.

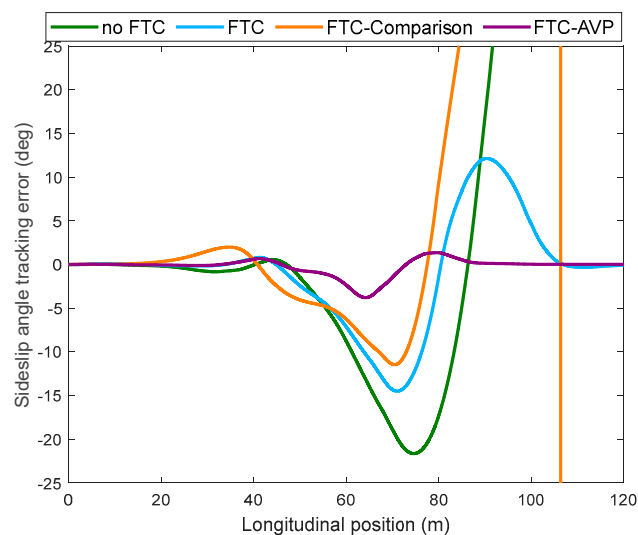


Figure 7. Sideslip angle tracking error in DLC under fault 1-3-4.

Figures 10 and 11 show the target and actual velocities with and without AVP. The initial target speed is 80 km/h, the highest speed that can safely track DLC conditions in a fault-free state. However, when actuator faults are complex and severe, continuing to use the original velocity target exceeds the capability boundary of FTC, resulting in suboptimal trajectory tracking. The actual average vehicle speed under the FTC-AVP is about 65 km/h, only 5 km/h lower than the maximum safe tracking speed of 70 km/h obtained through continuous squeeze tests. This not only ensures safety but also maximizes the vehicle operational flexibility, achieving ideal trajectory tracking control and demonstrating the effectiveness of our proposed strategy.

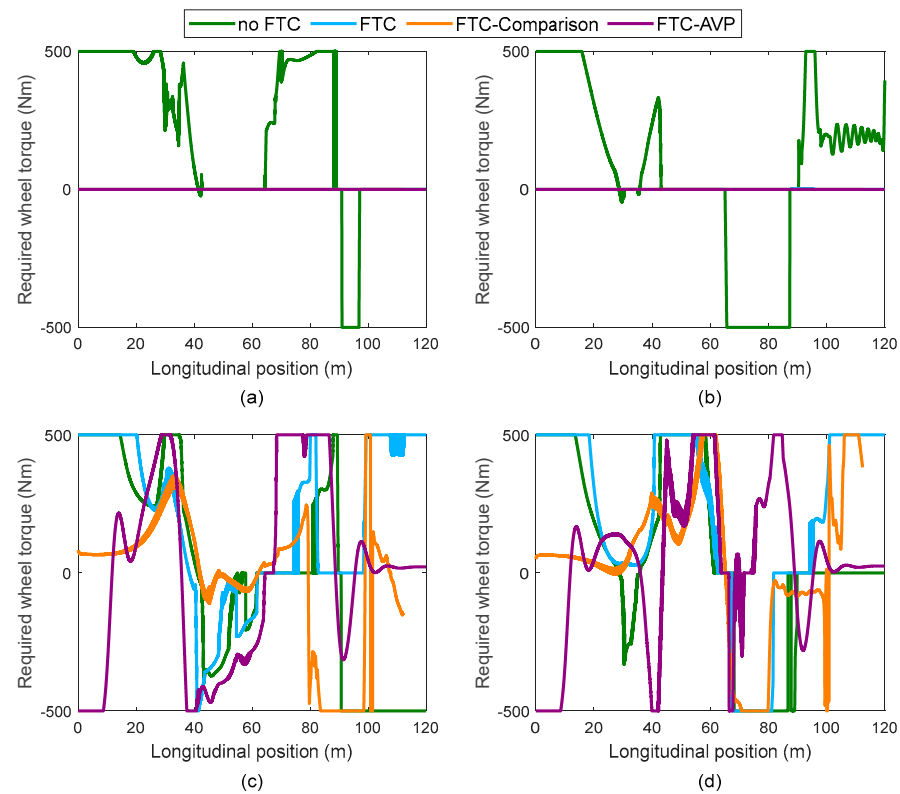


Figure 8. Four-wheel torque commands under four control strategies. (a) Front left wheel. (b) Front right wheel. (c) Rear left wheel. (d) Rear right wheel.

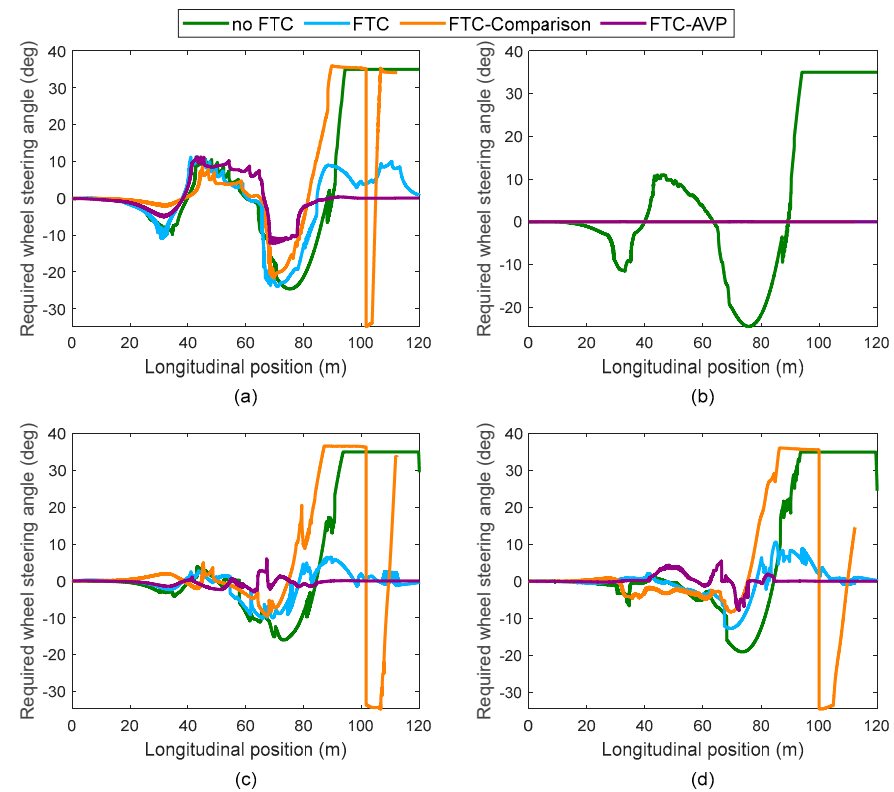


Figure 9. Four-wheel steering angle commands under four control strategies. (a) Front left wheel. (b) Front right wheel. (c) Rear left wheel. (d) Rear right wheel.

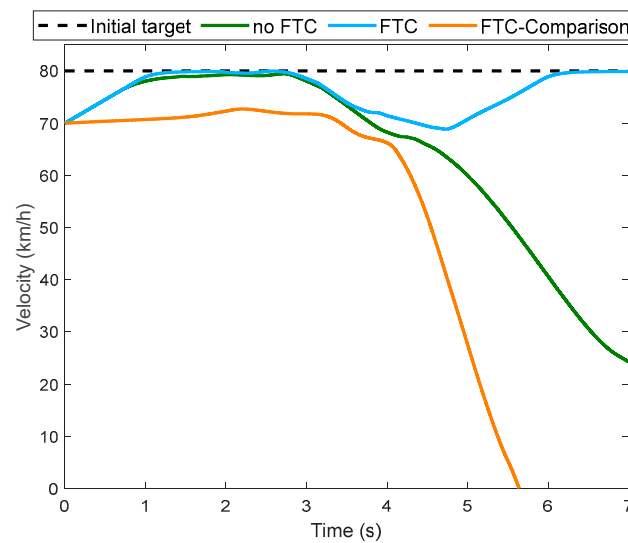


Figure 10. Target and actual velocities under no AVP.

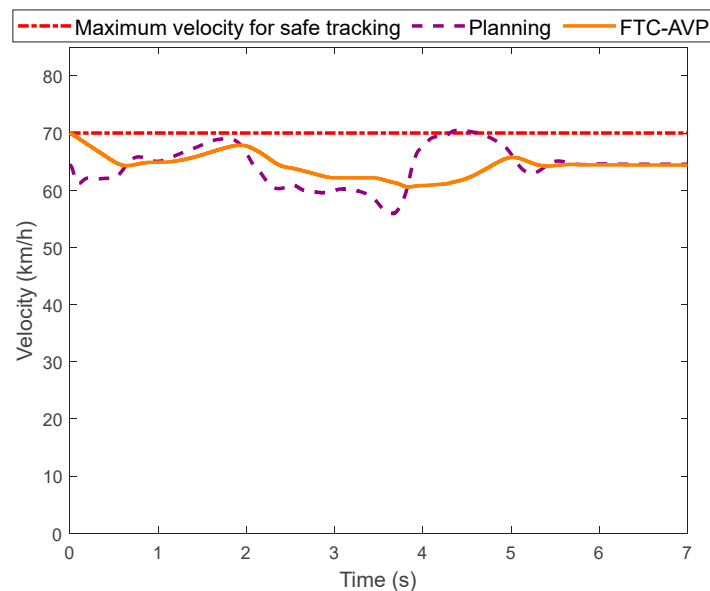


Figure 11. Target and actual velocities under AVP.

5.2. Comparison under Various Fault Types

In this section, we thoroughly analyze the FTC performance of 4WID-4WIS vehicles across all fault types under DLC conditions. The DLC trajectory tracking performance without FTC is illustrated in Figure 12.

The vehicle's front and rear axles are represented on the horizontal and vertical axes, respectively. From left to right, the actuators are organized as left-wheel drive, steering, right-wheel drive, and steering. A value of 1 signifies a functional actuator, while 0 indicates a complete failure. For example, "1011-1111" means the steering actuator on the front left wheel has completely failed, while the other seven actuators remain functional. "D" denotes the drive actuator, and "S" represents the steering actuator, with fault situations arranged according to the number of front-axle drive and steering failures. During the DLC maneuver, we compare trajectory tracking errors e_ϕ , e_y , e_β , and e_v to the non-failure condition, normalize the results by averaging the reciprocals, and use this as the control effectiveness score. A score of 0 is assigned when the DLC cannot be completed. Without FTC, most actuator failures lead to loss of control and failure to complete the DLC trajectory. Only in the case where the front-axle steering remains functional and at least one of the

four-wheel drives is still operational can good trajectory tracking control be achieved without FTC. This suggests that rear-wheel steering or partial drive actuator failures are not critical in this condition but rather contribute to improved vehicle handling stability.

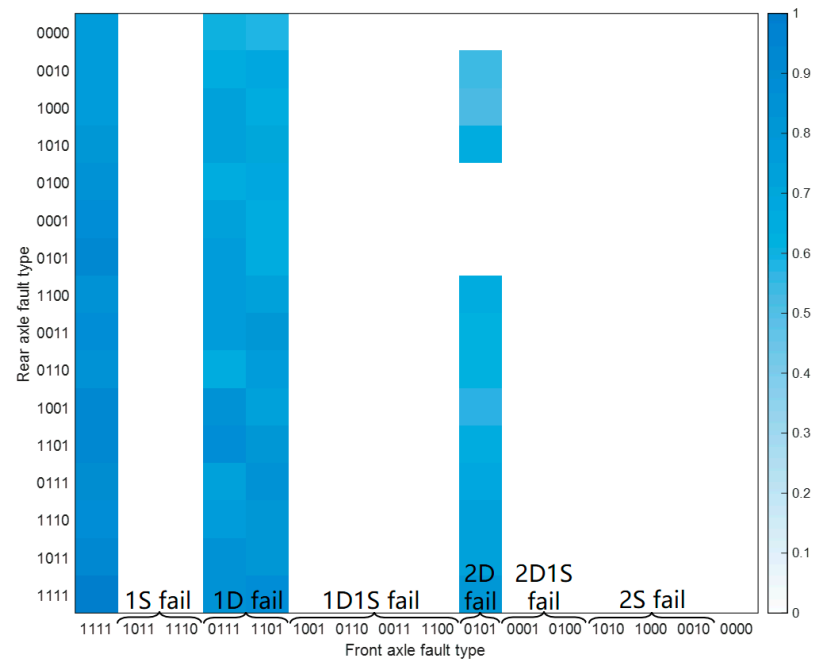


Figure 12. The DLC trajectory tracking performance under no FTC.

Figure 13 shows the DLC trajectory tracking performance with the referenced FTC. While it can maintain vehicle stability under FTC, its performance declines as the number of actuator failures increases and the fault scenarios become more complex. The control effectiveness scores under FTC-Comparison are generally lower than those achieved by the proposed FTC. In many cases, it fails to complete DLC trajectory tracking, such as the “fault 1-3-4” scenario mentioned in Section 5.1, labeled as “0100-1111” in Figure 13.

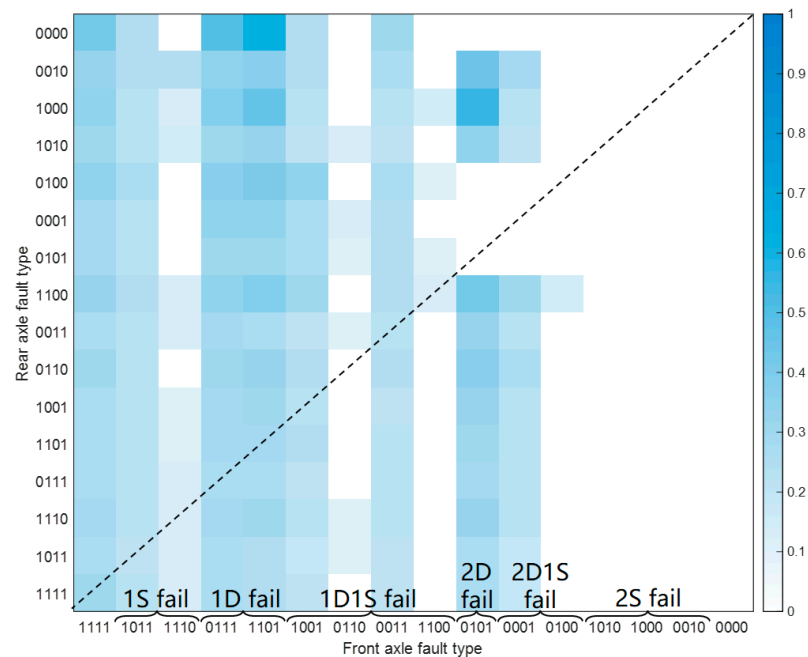


Figure 13. The DLC trajectory tracking performance under FTC-Comparison.

Figure 14 shows the DLC trajectory tracking performance with the proposed FTC. The FTC strategy, which reallocates control and efficiently utilizes the remaining functional actuators, significantly increases the number of fault scenarios where the DLC can be successfully completed, especially in cases of single front-wheel steering failure. However, front-axle steering failures still present challenges for DLC tracking, while some rear-axle steering failures are manageable. Generally, rear-wheel steering failures demonstrate better FTC than front-wheel steering failures. However, due to the reduced attainable force range under fault conditions, FTC cannot always achieve the performance seen in a fault-free state, necessitating a potential reduction in the target vehicle velocity.

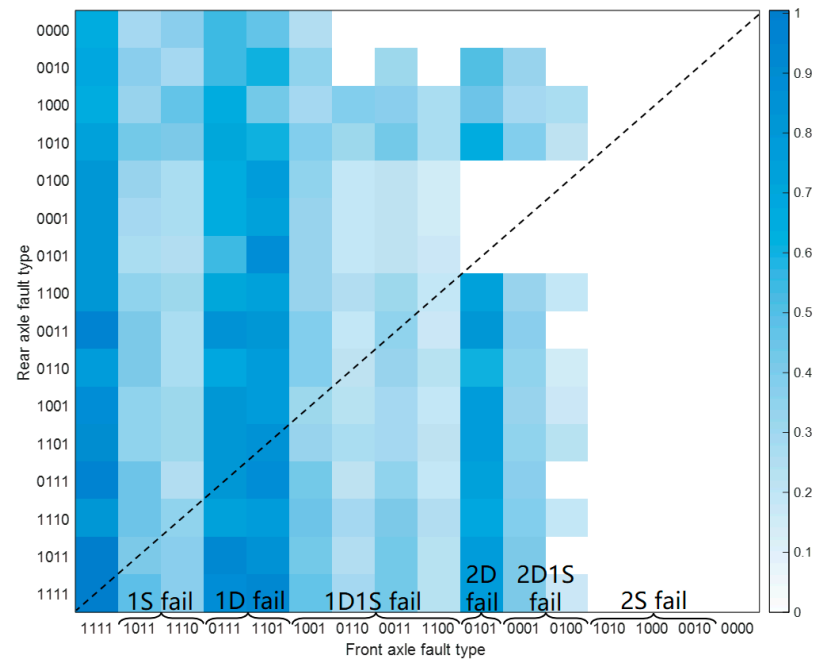


Figure 14. The DLC trajectory tracking performance under FTC.

Figure 15 depicts the DLC trajectory tracking performance under FTC-AVP. Nearly all fault types allow for successful DLC trajectory tracking, with better control scores compared to the scenarios without AVP. The AVP results in an average speed approximately 6 km/h lower than the maximum safe speed determined through continuous squeeze testing, showcasing the effectiveness of our proposed control strategy. This approach balances vehicle safety and maneuverability, maximizing overall performance. Nevertheless, there are still 30 situations where DLC cannot be completed: 16 cases involve complete four-wheel drive failure, and 14 involve complete four-wheel steering failure with fewer than four functional drive wheels. In these scenarios, no control strategy can restore vehicle control, necessitating a complete stop and rescue.

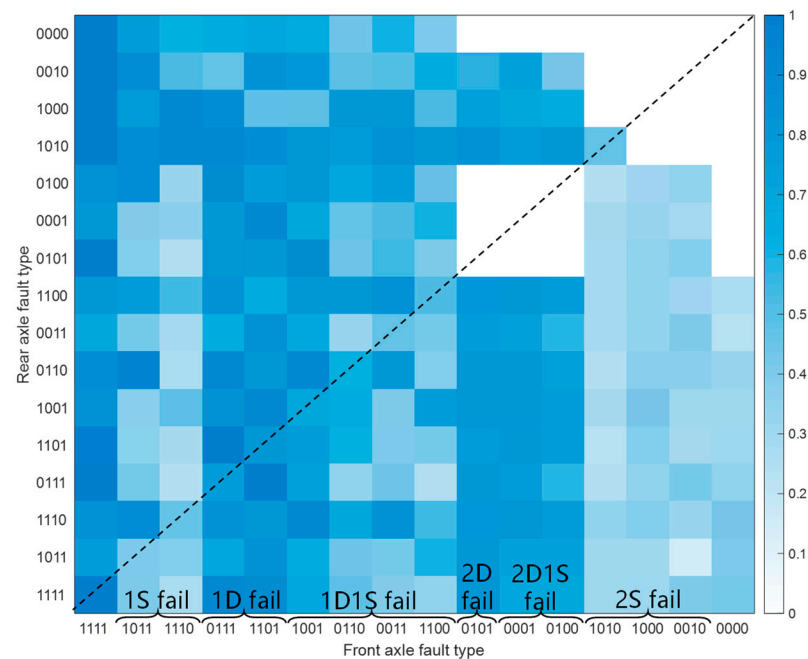


Figure 15. The DLC trajectory tracking performance under FTC-AVP.

6. Conclusions

In this paper, a hierarchical active fault-tolerant controller is proposed, significantly enhancing vehicle safety and maneuverability in the presence of actuator faults. The required resultant force is determined by the upper-level motion controller based on trajectory tracking error feedback, while the middle-level control allocation optimally distributes tire forces to fault-free lower-level actuators through constraint optimization, informed by fault diagnosis. Additionally, the vehicle attainable force domain under various actuator fault conditions is calculated using SVD, and a fault tolerance index is introduced to define the vehicle fault tolerance boundary. Building on this, a computationally efficient AVP strategy is developed to dynamically adjust to fault conditions. The proposed strategy is validated across all fault scenarios, demonstrating improved safety under fault conditions while maximizing the vehicle's maneuverability compared to existing methods, representing a significant advancement in FTC systems. The fault tolerance index, derived from the SVD of a matrix, simplifies the calculation of the vehicle attainable force domain, significantly reducing computational costs and improving real-time performance. Furthermore, it provides a reliable basis for quantifying and classifying fault severity.

In future work, we plan to conduct real-vehicle experiments to further validate the effectiveness of the control strategy and explore ways to optimize and improve the real-time performance of the control algorithm.

Author Contributions: Conceptualization, A.L.; methodology, A.L.; software, A.L.; validation, A.L.; writing—original draft preparation, A.L.; writing—review and editing, A.L.; supervision, G.T. All authors have read and agreed to the published version of the manuscript.

Funding: This research was funded by the National Natural Science Foundation of China (Grant No.52272372) and Beijing Natural Science Foundation (3224064).

Data Availability Statement: The data presented in this study are available on request from the corresponding author.

Conflicts of Interest: The authors declare no conflicts of interest.

References

1. Lu, Y.; Li, G.; Yue, Y.; Wang, Z. Fault Detection and Data-driven Optimal Adaptive Fault-tolerant Control for Autonomous Driving using Learning-based SMPC. *IEEE Trans. Intell. Veh.* **2024**, 1–15. [\[CrossRef\]](#)
2. Hu, C.; Wei, X.; Ren, Y. Passive fault-tolerant control based on weighted LPV tube-MPC for air-breathing hypersonic vehicles. *Int. J. Control Autom. Syst.* **2019**, 17, 1957–1970. [\[CrossRef\]](#)
3. Chen, T.; Chen, L.; Xu, X.; Cai, Y.; Jiang, H.; Sun, X. Passive actuator-fault-tolerant path following control of autonomous ground electric vehicle with in-wheel motors. *Adv. Eng. Softw.* **2019**, 134, 22–30. [\[CrossRef\]](#)
4. Abzi, I.; Kabbaj, M.; Benbrahim, M. Design of Fractional Order Sliding Mode Controller for Lateral Dynamics of Electric Vehicles. In Proceedings of the 2nd International Conference on Electronic Engineering and Renewable Energy Systems, ICEERE 2020, Saidia, Morocco, 13–15 April 2020.
5. Lu, A.; Li, R.; Xu, Y.; Tian, G. Adaptive Fault-Tolerant Control for 4WID-4WIS Electric Vehicles under Steering System Failures. In Proceedings of the 36th Chinese Control and Decision Conference, IEEE CCDC 2024, Xi'an, China, 25–27 May 2024.
6. Huang, C.; Naghdy, F.; Du, H. FDI Based Fault-Tolerant Control for Steer-by-Wire Systems. In Proceedings of the 2018 IEEE Conference on Control Technology and Applications (CCTA), Copenhagen, Denmark, 21–24 August 2018.
7. Zhang, D.; Liu, G.; Zhou, H.; Zhao, W. Adaptive sliding mode fault-tolerant coordination control for four-wheel independently driven electric vehicles. *IEEE Trans. Ind. Electron.* **2018**, 65, 9090–9100. [\[CrossRef\]](#)
8. Luo, Y.; Hu, Y.; Jiang, F.; Chen, R.; Wang, Y. Active fault-tolerant control based on multiple input multiple output-model free adaptive control for four wheel independently driven electric vehicle drive system. *Appl. Sci.* **2019**, 9, 276. [\[CrossRef\]](#)
9. Wang, J.; Longoria, R.G. Coordinated and Reconfigurable Vehicle Dynamics Control. *IEEE Trans. Control Syst. Technol.* **2009**, 17, 723–732. [\[CrossRef\]](#)
10. Cui, G.; Bao, C.; Guo, M.; Xu, Y.; He, Y.; Wu, J. Research on Path Tracking Fault-Tolerant Control Strategy for Intelligent Commercial Vehicles Based on Brake Actuator Failure. *Actuators* **2024**, 13, 97. [\[CrossRef\]](#)
11. Zhu, S.; Li, H.; Wang, G.; Kuang, C.; Chen, H.; Gao, J.; Xie, W. Research on Fault-Tolerant Control of Distributed-Drive Electric Vehicles Based on Fuzzy Fault Diagnosis. *Actuators* **2023**, 12, 246. [\[CrossRef\]](#)
12. Deng, H.; Zhao, Y.; Nguyen, A.T.; Huang, C. Fault-Tolerant Predictive Control With Deep-Reinforcement-Learning-Based Torque Distribution for Four In-Wheel Motor Drive Electric Vehicles. *IEEE/ASME Trans. Mechatron.* **2023**, 28, 668–680. [\[CrossRef\]](#)
13. Dai, H.; Chen, P.; Yang, H. Fault-Tolerant Control of Skid Steering Vehicles Based on Meta-Reinforcement Learning with Situation Embedding. *Actuators* **2022**, 11, 72. [\[CrossRef\]](#)
14. Mihály, A.; Gáspár, P. Reconfigurable Fault-Tolerant Control of In-Wheel Electric Vehicles with Steering System Failure. *IFAC-PapersOnLine* **2015**, 48, 49–54. [\[CrossRef\]](#)
15. Zhang, Y.; Lu, G. Research on control method of four-wheel-independent-driving system based on X-by-wire chassis. In Proceedings of the China SAE Congress 2020: Selected Papers, Singapore, 13 January 2022.
16. Liu, Y.; Zong, C.; Zhang, D.; Zheng, H.; Han, X.; Sun, M. Fault-tolerant control approach based on constraint control allocation for 4WIS/4WID vehicles. *Proc. Inst. Mech. Eng. Part D J. Automob. Eng.* **2021**, 235, 2281–2295. [\[CrossRef\]](#)
17. Zhu, M.; Wang, Y.; Pu, Z.; Hu, J.; Wang, X.; Ke, R. Safe, efficient, and comfortable velocity control based on reinforcement learning for autonomous driving. *Transp. Res. Part C Emerg. Technol.* **2020**, 117, 102662. [\[CrossRef\]](#)
18. Herrmann, T.; Wischnewski, A.; Hermansdorfer, L.; Betz, J.; Lienkamp, M. Real-time adaptive velocity optimization for autonomous electric cars at the limits of handling. *Trans. Intell. Veh.* **2020**, 6, 665–677. [\[CrossRef\]](#)
19. Pacejka, H. *Tire and Vehicle Dynamics*, 3rd ed.; Elsevier: Philadelphia, PA, USA, 2012; pp. 100–112.
20. Ono, E.; Hattori, Y.; Muragishi, Y.; Koibuchi, K. Vehicle dynamics integrated control for four-wheel-distributed steering and four-wheel-distributed traction/braking systems. *Veh. Syst. Dyn.* **2006**, 44, 139–151. [\[CrossRef\]](#)
21. Goh, J.Y.M. Automated Vehicle Control Beyond the Stability Limits. Ph.D. Thesis, Stanford University, Stanford, CA, USA, 2019.
22. De Castro, R.; Tanelli, M.; Araújo, R.E.; Savaresi, S.M. Design of safety-oriented control allocation strategies for overactuated electric vehicles. *Veh. Syst. Dyn.* **2014**, 52, 1017–1046. [\[CrossRef\]](#)
23. Li, B.; Lin, C.; Ahmadi, J.; Siampis, E.; Longo, S.; Velenis, E. An integrated path-tracking and control allocation method for autonomous racing electric vehicles. *Veh. Syst. Dyn.* **2024**, 62, 1517–1540. [\[CrossRef\]](#)
24. Fors, V.; Olofsson, B.; Nielsen, L. Attainable force volumes of optimal autonomous at-the-limit vehicle manoeuvres. *Veh. Syst. Dyn.* **2020**, 58, 1101–1122. [\[CrossRef\]](#)

Disclaimer/Publisher's Note: The statements, opinions and data contained in all publications are solely those of the individual author(s) and contributor(s) and not of MDPI and/or the editor(s). MDPI and/or the editor(s) disclaim responsibility for any injury to people or property resulting from any ideas, methods, instructions or products referred to in the content.